

Analytical Model of Transpired-Coolant Concentration at Downstream Wall in High-Speed Laminar Flow

Hassan Saad Ifti^{*}, Tobias Hermann[†], and Matthew McGilvray[‡]
University of Oxford, Oxford, OX2 0ES, United Kingdom

An analytical model based on one-dimensional diffusion is proposed to predict the mixing between the coolant gas and boundary-layer gas at the wall downstream of a transpiring injector in a laminar flow. The model is validated against coolant concentration data experimentally obtained at Mach 7 over a flat-plate at zero pressure gradient. It successfully predicts the mixing at the wall downstream within 17% of the experimental data. It is shown that this mixing mechanism at the wall in laminar flows is fully described by the process of diffusion. The coolant coverage at a given downstream location is promoted when the stream-wise velocity decreases, the blowing ratio increases, or the diffusion coefficient drops. Finally, a mass budget calculation is performed for a transpiration-cooled hypersonic vehicle employing the analytical model. The model predicts a 3.6 times less coolant mass requirement when helium is used as the coolant gas as opposed to nitrogen for the chosen trajectory. However, helium requires twice the storage volume compared to nitrogen.

Nomenclature

A	= area of porous injector, m^2
b	= leading-edge span, m
C	= non-dimensional coolant concentration, –
C_0	= initial non-dimensional coolant concentration, –
C_w	= non-dimensional coolant concentration at the wall, –
D, D_{12}	= diffusion coefficient for binary mixture, m^2/s
F	= blowing ratio, –
h	= coolant's initial slab height, m
h'	= coolant's initial slab height excluding entrained mass from boundary-layer gas, m
m_c	= required coolant mass, kg

^{*}DPhil Candidate, Oxford Thermofluids Institute, Department of Engineering Science, University of Oxford, Southwell Building, Osney Mead.
Email: saad.ifti@eng.ox.ac.uk

[†]Lecturer, Oxford Thermofluids Institute, Department of Engineering Science, University of Oxford, Southwell Building, Osney Mead.

[‡]Associate Professor, Oxford Thermofluids Institute, Department of Engineering Science, University of Oxford, Southwell Building, Osney Mead.

$m_{c,t}$	=	total required coolant mass over full flight duration, kg
\dot{m}_c	=	required coolant mass flow rate, kg/s
M_{air}	=	molar mass of air, g/mol or kg/mol
M_c	=	molar mass of coolant gas, g/mol or kg/mol
p	=	pressure, Pa
p_0	=	stagnation pressure, MPa
p_e	=	boundary-layer edge pressure, Pa
$p_{\text{O}_2, \text{air}}$	=	oxygen partial pressure with air injection, Pa
$p_{\text{O}_2, \text{foreign gas}}$	=	oxygen partial pressure with foreign gas injection, Pa
p_{storage}	=	pressure for coolant gas storage, bar or Pa
Q_{storage}	=	volume required to store total required coolant gas, m ³
r_{12}	=	binary collision diameter, Å
R_G	=	universal gas constant, J · K ⁻¹ · mol ⁻¹
Re_{cell}	=	cell Reynolds number, –
Re_s	=	Reynolds number based on injector length s , –
Re_u	=	unit Reynolds number, m ⁻¹
s	=	injector length, m
t	=	time, s
t_{flight}	=	flight duration, s
T	=	temperature, K
T_0	=	total temperature, K
T_c	=	coolant temperature, K
T_e	=	boundary-layer edge static temperature, K
T_{storage}	=	coolant storage temperature, K
T_w	=	wall temperature, K
u_c	=	coolant velocity, m/s
u_e	=	boundary-layer edge velocity, m/s
x	=	distance from leading edge, m
x_0	=	distance from leading edge to injector end, m
x'	=	distance downstream of injector, m
X_{N_2}	=	mole fraction of nitrogen, –
$X_{\text{N}_2,e}$	=	mole fraction of nitrogen at boundary-layer edge, –

y	= wall-normal distance, m
δ_{ent}	= additional slab height due to entrained boundary-layer gas, m
ζ	= driving parameter, –
η_c	= concentration effectiveness, –
μ_e	= boundary-layer edge viscosity, Pa · s
ρ_c	= coolant density, kg/m ³
ρ_e	= boundary-layer edge density, kg/m ³
τ	= time, s

I. Introduction

High-speed vehicles are prone to high heat fluxes due to aerodynamic heating [1, 2]. Passive, semi-passive, and active cooling methods are available options to mitigate this heating. Amongst the active cooling methods, transpiration cooling is a promising technology that could enhance the re-usability of vehicle parts that are subject to high peak heating such as leading edges or control-fin joints. It would protect the vehicle from both heat and oxidation, acting as a dual-mode protection system. This cooling process consists of three different subprocesses [3] (see Fig. 1): (a) heat from the wall is convected out by the coolant gas; (b) the coolant gas creates a film (blue) that insulates the wall underneath from the hot cross-flow; and (c) the coolant film protects the wall from free-stream oxygen and thereby prevents oxidation of the wall, which enables the wall material to operate at a higher temperature enhancing radiative cooling [4] and reduces recombination heating [5]. The success of the latter two processes depends on the coolant film that is formed on and downstream of the injector. The concentration of this protective film reduces in the stream-wise direction and eventually the film diminishes at a downstream location as it mixes with the incoming boundary-layer gas (see the concentration gradient, $C(x, y)$ in Fig. 1). The concentration of the film is 100% if no mixing takes place (full coverage of coolant gas, e.g. helium or nitrogen) and 0% when fully diminished.

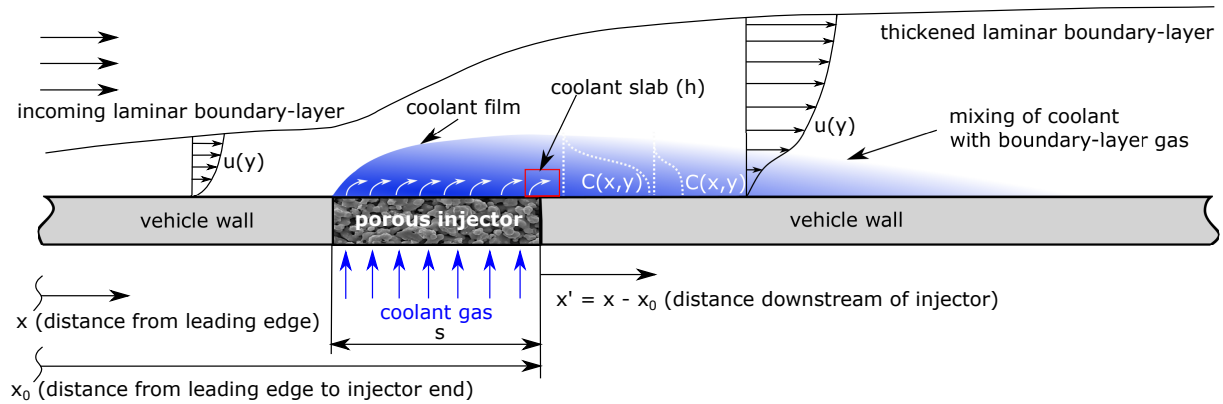


Fig. 1 Schematic of a flat surface with a porous, transpiration cooling injector (not to scale).

The majority of the studies available in the literature are concerned with a common goal of understanding – and in some cases predicting – the mixing between the coolant gas and the external cross-flow, both on and downstream of the injector. These studies primarily focus on mixing with respect to heat flux reduction. However, understanding the mixing in terms of coolant concentration – which is the central topic of this article – is necessary to enable the dual-mode protection that transpiration cooling offers, i.e. protection against oxidation in addition to its cooling capability. The downstream mixing is of particular interest because the coolant gas injected through the injector can be further utilised to protect the downstream parts from either heat, oxidation, or both. This reduces the required mass of coolant that needs to be carried in the vehicle. In addition, it can be used to protect parts that cannot be made porous due to their complexity or the high stresses they endure (e.g. the hinge that joins a control fin to the fuselage). Furthermore, this technique can be employed to protect optical windows on hypersonic vehicles by placing the injector upstream of the window [6, 7].

A considerably large body of work on downstream mixing spanning more than five decades is available in the literature [8, 9]. These studies range from mixing with respect to heat flux reduction at the wall to the aerodynamic effects [10–12]. The majority of studies, however, focus on turbulent flows only, mostly for film cooling applications in turbine blades and rocket nozzle walls. The flight trajectory of a high-speed vehicle, particularly a hypersonic vehicle, is not necessarily limited to turbulent flows and may span across all three flow regimes, i.e. laminar, transitional, and turbulent. Protecting these vehicles – either from heat or oxidation – in every flow regime could therefore become necessary. Furthermore, hypersonic vehicles could experience their highest peak heating in the laminar regime [13] due to the high re-entry speeds at high altitudes where the density of the atmosphere is considerably lower. In spite of this need, only a handful of studies on film cooling or transpiration cooling in laminar flows are available in the literature. In particular, the underlying mechanism behind laminar mixing in terms of the coolant concentration – a mechanism on which the success of oxidation protection depends – has not been identified.

Richards and Stollery [14] performed one of the first experimental studies involving laminar flows, where a tangential injection was introduced in a hypersonic boundary layer to cool a flat-plate at Mach 10. A discrete-layer theory based on heat conduction was proposed by the authors. Heufer and Olivier [15] developed a correlation factor using the energy equation similar to film cooling theory [8] but they replaced the turbulent velocity profile with a laminar one. This correlation factor was validated, both numerically and experimentally, employing a slot injector on a flat-plate in laminar, supersonic flows. In a subsequent experimental study by Hombsch and Olivier [16], the slot geometry and coolant gas were varied in supersonic flows. The authors showed that film cooling was more successful in laminar flows than in turbulent flows, and a correlation was developed for laminar flows. Keller et al. [17] conducted direct numerical simulations with different coolant gases and compared the numerical results to these experimental data. The authors achieved a relatively reasonable collapse of the simulated data for nine different gases by multiplying the correlation factor by the ratio of specific heat capacities of the gases raised to the power of $1/3$. They further performed

a parameter study to identify the dominant variables that affect the cooling downstream of the slot injector. The authors concluded that the effect of the diffusion coefficient on cooling effectiveness is negligible, whereas a change in the viscosity, thermal conductivity, density, molar mass, Prandtl number, or specific heat capacity of the coolant has a large impact on cooling. In addition, it was highlighted that extending the existing correlation factor – developed for a single-species mixture – for a binary-gas mixture (where the coolant gas and the boundary-layer gas are not identical) is difficult due to the large number of influencing variables. These studies, however, focus on heat flux reduction only, not the concentration of the coolant gas at the wall.

In a recent study, Ifti et al. [3] proposed a new correlation for laminar mixing based on experimental heat flux data obtained at flow conditions and coolant mass injection rates different from those in the study by Hombsch and Olivier [16]. The authors demonstrated that a universal correlation for laminar mixing – independent of flow conditions, the coolant gas, and injection rates – was not possible in the traditional approach used in film cooling theory due to the fundamental difference in the mixing mechanism in laminar boundary layers in absence of turbulent mixing. The Reynolds analogy between heat and mass transfer [18] does not apply to laminar flows (the ratio of Schmidt number and Prandtl number is not equal to unity). Therefore, the concentration distribution of the coolant gas at the wall becomes a compelling quantity for understanding the mixing process in laminar boundary layers.

Furthermore, Ifti et al. [3] – by experimentally obtaining spatially-resolved concentration data – demonstrated that the cooling effectiveness is not only affected by the thermal properties of the coolant gas but also by its physical form and trace, i.e. concentration. For instance, it is widely known that helium is a better coolant than nitrogen because of helium's higher heat capacity; however, at a given coolant mass flux, helium also forms a more formidable film due to its seven times higher volumetric flow rate compared to that of nitrogen. This phenomenon has been discussed by Gülhan and Braun [19], Keller et al. [17], and Hombsch and Olivier [16] as well. It is therefore necessary to understand the formation and mixing of the physical film, predict the coolant concentration, and identify the variables that drive the mixing with respect to the coolant's concentration.

The coolant's concentration is a key parameter for designing an oxidation protection system. Oxidation protection or reduction can allow certain materials, such as ultra-high-temperature ceramics (UHTCs), to operate at temperatures above 3000 K without failing as experimentally shown by Ewenz Rocher et al. [5]. A high operational temperature would enable a higher amount of passive radiative cooling [4]. In addition, predicting the ratio of the coolant gas and the boundary-layer gas can help improve the current film cooling correlations for laminar flows. Most correlations or correlation factors for laminar film cooling in the literature are based on the assumption of a fully mixed gas mixture (e.g. Heufer and Olivier [15]), which is not the case in a laminar boundary layer. The correct prediction of the ratio of gases becomes particularly important in cases where the coolant gas properties are significantly different from those of the boundary-layer gas, e.g. helium injection in air. To the authors' knowledge, no model exists in the open literature to date that describes this mixing process with respect to the concentration of the coolant at the wall in a laminar boundary layer.

In this article, an analytical model based on one-dimensional diffusion is proposed to describe this mixing process and predict the coolant concentration at the wall downstream of the injector. The model is validated against experimentally obtained coolant concentration data at the wall downstream of a porous injector on a flat-plate at zero pressure gradient in a laminar, Mach 7 flow (reported in Ref. [3]). This is the first time an analytical model is reported to describe the mixing mechanism between the coolant and the boundary-layer gas with respect to coolant concentration at the wall in a laminar flow.

II. Methodology

A. Analytical Model

The fluid downstream of the injector is modelled as a moving slab (annotated in red in Fig. 1) of a binary gas composition that advects downstream at the boundary-layer edge velocity, $u_e = x'/t$, where t is time. It is assumed that the coolant gas diffuses in the wall-normal direction, y , as the slab advects downstream. A solution for the coolant concentration at the wall, i.e. at $y = 0$, is sought as a function of the downstream distance, $x' = x - x_0$.

The one-dimensional, unsteady diffusion equation is given as

$$\frac{\partial C}{\partial t} = D \frac{\partial^2 C}{\partial y^2}, \quad (1)$$

where C is the non-dimensional concentration of the coolant gas ($C \in [0, 1]$) and D is the diffusion coefficient [20]. The coordinate y denotes the wall-normal direction. With time, $t = x'/u_e$, a solution to Eq. (1) is an error function according to Crank [20] expressed as

$$\frac{C(x', y)}{C_0} = \frac{1}{2} \left[\operatorname{erf} \left(\frac{h - y}{\sqrt{4Dx'/u_e}} \right) + \operatorname{erf} \left(\frac{h + y}{\sqrt{4Dx'/u_e}} \right) \right], \quad [y \geq 0]. \quad (2)$$

Here, x' is the downstream distance (see Fig. 1), u_e is the stream-wise, boundary-layer edge velocity, and C_0 and h respectively denote the initial coolant concentration (maximum value 1 or 100%) and initial height of the coolant slab at $x' = 0$, i.e. immediately downstream of the injector (h is defined and modelled in Section (II.B)). The downstream distance can be expressed in terms of the distance from the leading edge, x , as $x' = x - x_0$, where x_0 is the length from the leading edge to the injector end. At the wall, i.e. at $y = 0$, Eq. (2) reduces to

$$\eta_c = C(x, 0) = C_0 \operatorname{erf} \left(\sqrt{\frac{u_e h^2}{4D(x - x_0)}} \right) = C_0 \operatorname{erf}(\zeta), \quad [x - x_0 > 0]. \quad (3)$$

Equation (3) is the concentration effectiveness at the wall (not to be confused with the thermal film cooling effectiveness η or η_{th} , commonly used in the literature). A value of $\eta_c = 1$ denotes a full coolant film coverage, whereas a value of

$\eta_c = 0$ refers to a fully diminished coolant film. A driving parameter is defined as ζ . The diffusion coefficient, D , is calculated for a binary gas mixture (boundary-layer gas, 1, to coolant gas, 2) defined as

$$D = D_{12} = 0.0018583 \times T^{3/2} \sqrt{\frac{1}{M_1} + \frac{1}{M_2}} \frac{101325 \times 10^{-4}}{r_{12}^2 \sigma_{12} p}, \quad (4)$$

where M , r , and σ are respectively the molar mass, binary collision diameter, and temperature dependent collision integral [21]. D is evaluated at boundary-layer edge static pressure, $p = p_e$, and the wall temperature, $T = T_w$.

The initial concentration does not necessarily start at 1 immediately downstream of the injector, i.e. at $x' = 0$; it is a function of the injected coolant mass flux, injector type, and mixing between the coolant gas and boundary-layer gas on top of the injector. For this study, the value of C_0 is experimentally determined (see Section II.D); however, it could be determined by numerical simulations or future analytical models. The remaining quantity that is required is the initial slab height, h . A separate model is proposed to find h in the following section.

B. Model for Initial Slab Height

A schematic of the coolant slab height is illustrated in Fig. 2. At $x' = 0$, the slab height has the highest concentration. As the slab travels downstream, the concentration distribution becomes wider with its peak dropping (see profiles at $x' = x_1$ and $x' = x_2$).

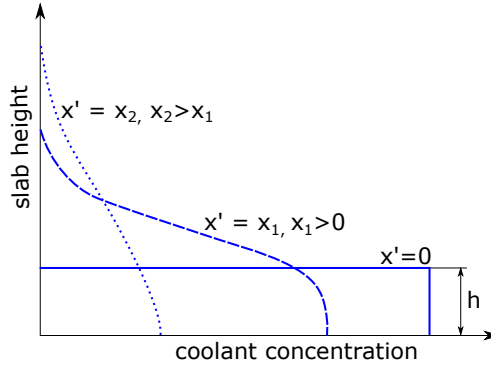


Fig. 2 Schematic of slab height distribution.

A simple model is constructed to obtain the slab initial height, h . This height is defined as

$$h = h' + \delta_{\text{ent}}. \quad (5)$$

h' is obtained from the continuity equation across the control volume presented in Fig. 3 (blue, dashed line). The continuity equation yields

$$\begin{aligned} \rho_c u_c s &= \rho_c u_e h' \\ \Rightarrow h' &= \frac{u_c}{u_e} s, \end{aligned} \quad (6)$$

where s is the injector's stream-wise length and the subscripts e and c respectively denote boundary-layer edge and coolant quantities. It is assumed that the coolant reaches the edge velocity, u_e , after becoming tangential to the wall (shown in blue in Fig. 3) and obtains a height of h' at the end of the injector.

By substituting the blowing ratio, $F = (\rho_c u_c)/(\rho_e u_e)$, in Eq. (6), the following expression for h' is obtained:

$$h' = \frac{\rho_e}{\rho_c} F s, \quad \left[\because \frac{u_c}{u_e} = \frac{\rho_e}{\rho_c} F \right]. \quad (7)$$

At the exit of the porous injector, the coolant is at the boundary-layer edge pressure, p_e , and wall temperature, T_w . According to the ideal gas law, the coolant and boundary-layer edge densities are respectively $\rho_c = \frac{M_c p_e}{R_G T_w}$ (assuming temperature equilibrium in the porous injector) and $\rho_e = \frac{M_{\text{air}} p_e}{R_G T_e}$, where R_G is the universal gas constant, M_c is the molar mass of the coolant gas, and M_{air} is the molar mass of the boundary-layer gas (in this instance, air). Substituting these two equations for ρ_c and ρ_e in Eq. (7) yields

$$h' = \frac{M_{\text{air}} T_w}{M_c T_e} F s. \quad (8)$$

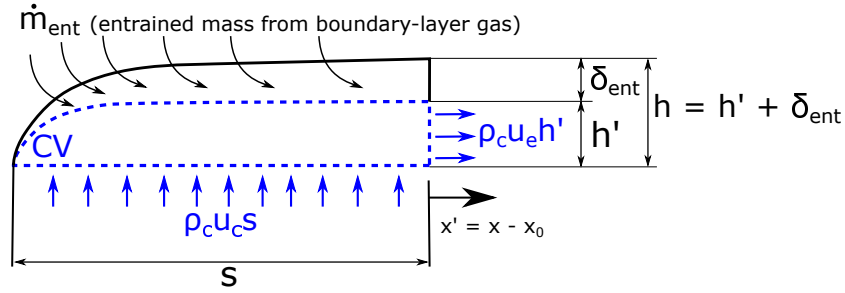


Fig. 3 Control volume around the injected gas and mass entrainment into the coolant gas over the injector.

The coolant gas mixes with the incoming boundary-layer gas over the injector and some boundary-layer gas is entrained into the coolant slab as shown in Fig. 3 (in black). The total slab height, h , is increased by the entrained mass, \dot{m}_{ent} , from the boundary layer. Similar to the entrained mass modelled in film cooling theory [8], it is assumed that this entrained mass grows as a boundary layer starting from the injector's starting point. Immediately downstream of the injector, this height becomes equivalent to the laminar boundary-layer thickness given as

$$\delta_{\text{ent}} = \frac{5s}{\sqrt{Re_s}} = 5 \sqrt{\frac{\mu_e s}{\rho_e u_e}}, \quad (9)$$

according to the Blasius solution [22], where, μ_e is the viscosity at the boundary-layer edge. Substituting Eq. (8) and

Eq. (9) in Eq. (5) yields the final equation for the slab height expressed as

$$h = \frac{M_{\text{air}} T_w}{M_c T_e} F s + 5 \sqrt{\frac{\mu_e s}{\rho_e u_e}}. \quad (10)$$

C. Numerical Simulations

To validate Eq. (10), two-dimensional simulations were performed employing the Thermochemical Implicit Non-Equilibrium Algorithm (TINA) – a Navier-Stokes solver developed by Fluid Gravity Engineering Ltd. TINA is a second-order accurate, point and line implicit, time marching algorithm. It employs the approximate Riemann solver in conjunction with flux limiters for the inviscid fluxes. A Total Variation-Diminishing (TVD) shock capturing algorithm was used, which ensures non-oscillatory behaviour near shock waves at essentially any free stream Mach number. Further details can be found in Refs. [23, 24].

A flow over the flat-plate geometry described in Section II.D was simulated (see Ref. [25] for details). A computational domain of $340 \text{ mm} \times 58 \text{ mm}$ was used with a total of 50511 grid points. The grid was equidistant in the stream-wise direction with step size of $\Delta x = 1 \times 10^{-3} \text{ m}$ and stretched in the wall-normal direction with a first cell height of $\Delta y = 2.5 \times 10^{-6} \text{ m}$. This resulted in a wall cell Reynolds number of $Re_{\text{cell}} < 1$, which ensured that the high gradients close to the wall were sufficiently resolved. A perfect gas model was selected. Air was chosen as the main flow gas. The flow conditions were matched with the conditions of the experiments stated in Section II.D.

Coolant injection was introduced in a fully converged base flow. At the wall, the nodes between 160 mm and 200 mm featured a permeable boundary condition, which was set as the mass flux of the coolant gas. Simulations for four cases of nitrogen injection with blowing ratios of $F = 0.0406\%$, $F = 0.0818\%$, $F = 0.153\%$, and $F = 0.295\%$, were performed. The mole fraction of nitrogen, X_{N_2} , in the flow field was extracted from the simulation results. A non-dimensional concentration quantity is defined as follows:

$$C(x, y) = \frac{X_{\text{N}_2}(x, y) - X_{\text{N}_2,e}}{1 - X_{\text{N}_2,e}}. \quad (11)$$

At locations where the mole fraction of nitrogen is identical to the value at the boundary-layer edge, i.e. $X_{\text{N}_2} = X_{\text{N}_2,e}$, the concentration is $C = 0$. On the other hand, a concentration of $C = 1$ would be possible at locations where the nitrogen mole fraction is exactly at unity, i.e. $X_{\text{N}_2} = 1$.

D. Experiments

The analytical model (Eq. 3) is validated against data obtained from transpiration cooling experiments conducted in a laminar flow employing a flat-plate model (see Fig. 4a) at Mach 7 in the Oxford High Density Tunnel (HDT) (see Ref. [3]). The flat-plate model was at an angle of attack of $\text{AoA} = 0^\circ$. A porous injector ($39.5 \text{ mm} \times 39.5 \text{ mm}$)

made of sintered zirconium diboride (ZrB_2) was situated 160 mm downstream of the leading edge. Thin-film gauges installed upstream and downstream of the injector measured the heat fluxes, which were compared to the correlation by Eckert [26] for laminar boundary layers to ensure that the boundary layer was laminar during the experiments. Pressure sensitive-paint (PSP) with an area of interrogation of $140 \text{ mm} \times 37 \text{ mm}$ was applied immediately downstream of the injector to measure the relative concentration of the injected coolant gas at the wall. The boundary-layer static pressure, temperature, and wall temperature were respectively $p_e = 542.04 \text{ Pa}$, $T_e = 43.53 \text{ K}$, and $T_w = 293 \text{ K}$. The total pressure, total temperature, and unit Reynolds number were $p_0 = 1.738 \text{ MPa}$, $T_0 = 470.1 \text{ K}$, and $Re_u = 12.9 \times 10^6 \text{ m}^{-1}$. The boundary-layer edge velocity was $u_e = 925.9 \text{ ms}^{-1}$. The blowing ratios (Cases 1 to 6) are given in Table 1. The coolant temperature, T_c , was equal to the wall temperature, T_w .

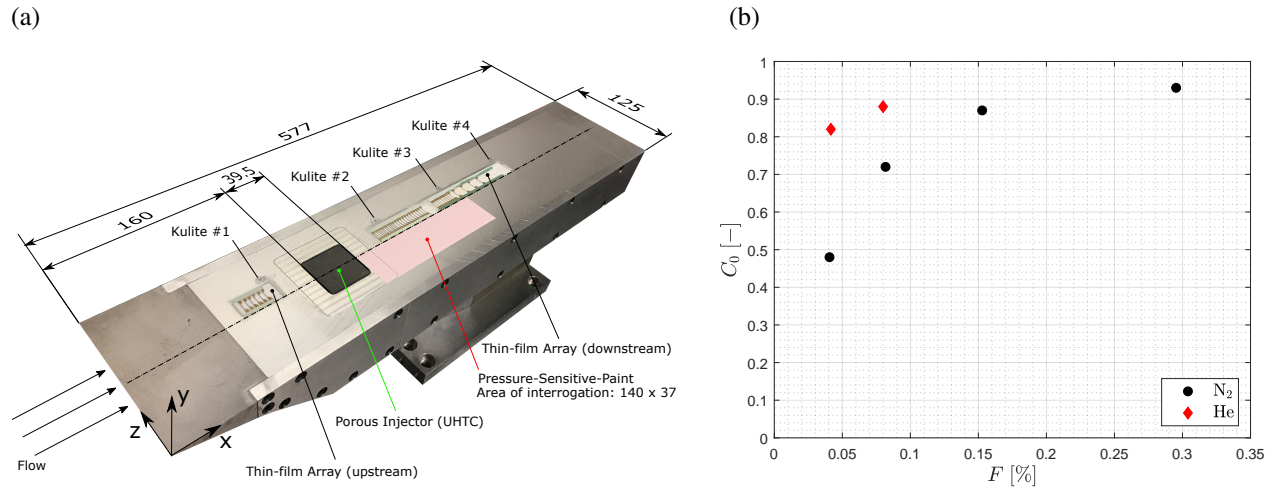


Fig. 4 (a) Flat-plate model with PSP coat downstream of the porous injector (reprinted with permission from Ifti et al. [3]; copyright 2022) and (b) experimentally obtained C_0 values as a function of F .

Table 1 Overview of blowing cases.

Case	1	2	3	4	5	6
F [%]	0.0406	0.0818	0.153	0.295	0.0416	0.08
Coolant gas	N_2	N_2	N_2	N_2	He	He

The PSP was excited by an LED of 390 nm and the emitted, higher wave length radiation was captured by a camera fitted with a red filter (550 nm). This excitation is quenched by oxygen in the air, and therefore the illumination can be calibrated by collecting illumination data for different flow static pressures (measured by surface mounted Kulite pressure transducers) without coolant injection. By applying the same calibration to cases with a foreign gas (coolant), a trace of the film can be identified as the quenching is influenced by the film. Injected coolant gas (nitrogen or helium) hinders the quenching by displacing air in the boundary layer. Comparing a case with air injection and one with a foreign gas injection at the same blowing ratio, gives a measure of how much air is displaced by the foreign gas, i.e. to

what extent the foreign gas is forming a film. The concentration film effectiveness is defined as

$$\eta_c = 1 - \frac{p_{O_2, \text{ foreign gas}}}{p_{O_2, \text{ air}}}, \quad (12)$$

where $p_{O_2, \text{ air}}$ and $p_{O_2, \text{ foreign gas}}$ are oxygen partial pressures with air and foreign gas injections, respectively, at the same blowing ratio.

A span-wise average of 10 mm close to the centreline – where the film is two dimensional and uninfluenced by the Mach angle – is taken to reduce the data for η_c to one dimension, which varies only in the stream-wise direction, x . The value of η_c immediately downstream of the injector is taken as the initial concentration, C_0 , for this study, i.e. $C_0 = \eta_c(x' = 0)$. In Fig. 4b, the experimentally obtained C_0 values for all cases are plotted as a function of the blowing ratio, F .

III. Validation

1. Results: Initial Slab Height

To determine the effective initial slab height, concentration profiles are extracted from simulation data immediately downstream of the injector (after $x = 200$ mm), where the impermeable wall boundary condition, $\frac{\partial C}{\partial y}\bigg|_{y=0} = 0$, is satisfied. The profiles are plotted in Fig. 5a. Since these profiles are continuous and monotonic, it is difficult to pinpoint an exact slab height. The slab height is a height up to which the concentration remains close to the wall concentration, C_w , i.e. the concentration at $y = 0$. When compared with the analytical model (Eq. 10), satisfactory results were found (as shown in Fig. 5b) with the following criteria for h :

$$h = \begin{cases} y(C = 0.95C_w) & \text{for } C_w < 1, \\ y(C = 0.99C_w) & \text{for } C_w = 1. \end{cases} \quad (13)$$

The y locations for the slab height obtained from Eq. (13) are shown in Fig. 5a (diamond markers). It is not surprising that the criterion for h is different between cases that feature a full film coverage at the wall ($C_w = 1$) and those that do not ($C_w < 1$). As shown in Fig. 5a, the profile close to the wall is different for the highest blowing ratio case that has a wall coolant concentration of $C_w = 1$ compared to the lower blowing ratio cases. A wall coolant concentration of $C_w = 1$ represents an intact coolant film at the wall where no mixing has occurred. Thus, the effective initial slab height would be a height where the coolant concentration is approximately the same as the wall coolant concentration ($C(h) = 0.99C_w$). Figure 5b illustrates the match between the analytical model for the h presented in Eq. (10) and the simulation results for four different blowing ratios. This simple analytical model yields values for h within 10% of the values obtained by the simulation.

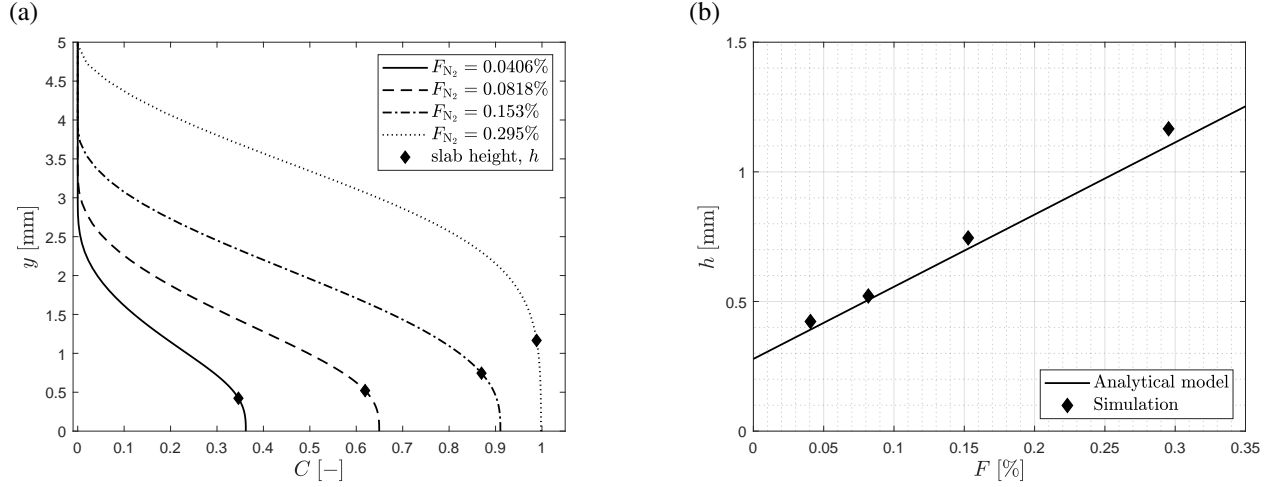


Fig. 5 (a) Coolant (nitrogen) concentration profiles obtained from simulation immediately downstream of injector (including slab height locations) and (b) slab height, h , as a function of F (analytical model, Eq. 10) versus simulation.

2. Results: Analytical Model

The results obtained from the analytical solution, i.e. Eq. (3), for Cases 1 to 6 are presented in Fig. 6a (dashed lines) along with the experimental data (solid lines). For all cases, the match between the analytical solution and the experimental data is encouragingly close, particularly considering the simplicity of the physical assumptions. At larger x values, a discrepancy can be noticed for Cases 3, 4, and 5. This deviation is attributed to the simplistic model (see Eq. 10) employed in this study for the slab height, h . However, this discrepancy is overall within 17% at the farthest downstream location, demonstrating the success of this simple model for h – even for helium injection. A perturbation of $\pm 10\%$ in h shifts this discrepancy to a maximum of 27% (for reference, the experimental uncertainty in η_c is within 5% [3]). This demonstrates how the difference in h obtained from TINA and the model could effect the final results and what the expected range of error is. The model for h , however, is successful in predicting the final results within 17% independent of the validation against TINA. The final results for η_c obtained from Eq. (3) not only capture the correct, monotonic trend farther downstream but also the plateau immediately downstream of the injector for cases with a higher blowing ratio, i.e. Cases 3, 4, and 6.

In Fig. 6b, a collapse of the experimental data for all cases is showcased with η_c/C_0 as a function of the driving parameter, $\zeta = \sqrt{\frac{u_e h^2}{4D(x-x_0)}}$. These collapsed data further demonstrate that the mixing mechanism at the wall can be described by Eq. (3). Figure 6b visualises the effect of change in the variables that are involved. As $\zeta \rightarrow \infty$, $\eta_c/C_0 \rightarrow 1$, and therefore film coverage of 1 can be achieved for higher ζ values (e.g. $\zeta > 2$). Since $\zeta \propto h \propto F$, a higher blowing ratio would result in a higher ζ value, i.e. a better film coverage, which is expected as long as a boundary-layer transition is not triggered. On the other hand, a higher diffusion coefficient, D , or larger x values would result in a lower ζ value, which would in return reduce the film coverage. According to Eq. (4), the diffusion coefficient is a function of temperature and pressure ($D \propto T^{3/2}$ and $D \propto 1/p$), and therefore flight conditions at high temperatures and low

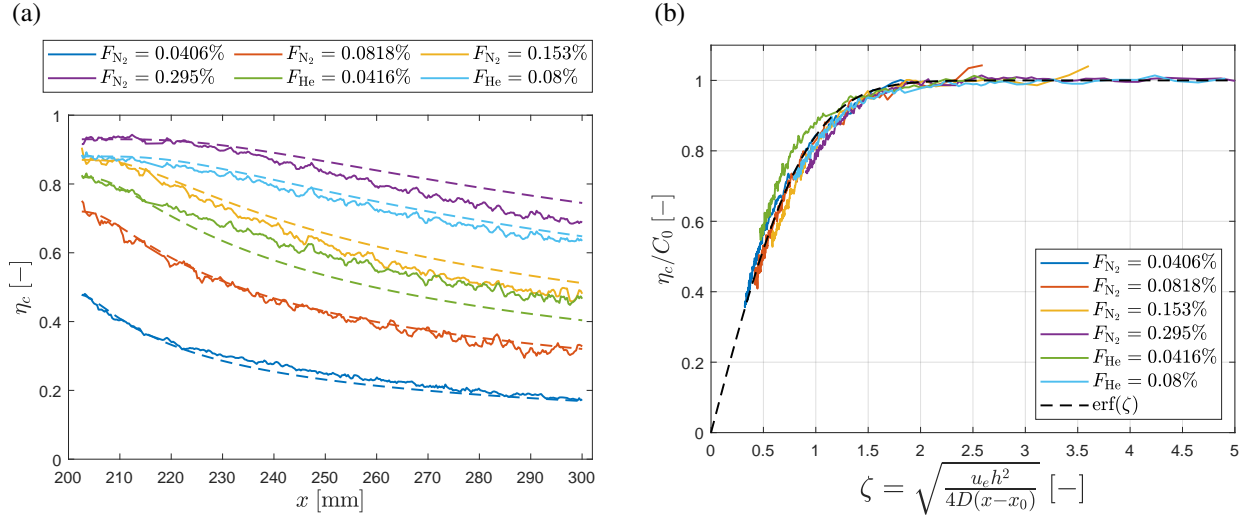


Fig. 6 Cases 1 to 6: (a) Concentration effectiveness, η_c , versus stream-wise direction, x (solid line: experimental data; dashed line: analytical model, Eq. (3) and (b) scaled concentration effectiveness, η_c/C_0 , versus driving parameter, ζ .

pressures would increase the diffusion coefficient.

According to Eq. (10), the first term in h is proportional to $1/u_e$ (since $F = (\rho_c u_c)/(\rho_e u_e)$) and the second to $1/\sqrt{u_e}$. In the numerator of ζ , the slab height, h , is multiplied by $\sqrt{u_e}$, and therefore the final relationship between the driving parameter and the stream-wise velocity becomes $\zeta \propto 1/\sqrt{u_e}$. If the air density remains constant and the vehicle accelerates, the edge mass flux, $\rho_e u_e$, would increase, resulting in a lower F and thus h . A higher stream-wise velocity would decrease ζ and thereby the film concentration, η_c .

The collapse of data presented in Fig. 6b further demonstrates that this analytical model correctly captures the effect of different coolant gases, in this case nitrogen and helium. In Ifti et al. [3] it was experimentally shown that helium forms a much more formidable film than nitrogen at the same blowing ratio due to helium's seven times larger volumetric flow compared to that of nitrogen. Keller et al. [17] reported this effect in their numerical investigation. This difference in volumetric flow rate for different gases at a given blowing ratio is taken into account in the first term of the right-hand side of Eq. (10).

The proposed model is only valid at the wall. The diffusion coefficient, D , is evaluated at the wall temperature, T_w . In the wall-normal direction, D would change due to the temperature gradient in the boundary layer. The assumption of a constant D made in Eq. (1) would not hold for the entire fluid in the wall-normal direction. In addition, the model assumes that the coolant is injected at the wall temperature, consistent with the experiments. This model is further limited to cases where the slab height, h , is close to or larger than the incoming boundary-layer thickness in order to assume that the slab reaches the edge velocity, u_e .

Overall, the results demonstrate that the mechanism of downstream mixing with respect to coolant concentration at the wall in a laminar boundary layer, where turbulent mixing is absent, is primarily driven by diffusion. The proposed

model (Eq. 3) can be used to determine the amount of coolant needed to protect a surface from oxidation in laminar conditions. In addition, this model provides the exact ratio of the coolant and the boundary-layer gas as a function of downstream distance, which can be utilised to approximate the thermal conductivity, density, viscosity, Prandtl number, molar mass, and specific heat capacity of the binary-gas mixture – quantities identified by Keller et al. [17] that influence cooling effectiveness – and improve the current models for predicting cooling effectiveness in laminar flows. Further, the ratio of the coolant and the boundary-layer gas obtained from this model can be incorporated in the correlation factor for cooling effectiveness proposed by Heufer and Olivier [15] to account for the laminar mixing of the two gases.

IV. Application

In a transpiration cooling system that is designed for application on a hypersonic vehicle, the coolant gas has to be carried inside the vehicle for a given mission, which would add to the total weight and volume of the vehicle. In addition, the reservoir and pipework required to store the coolant gas would increase the weight of the vehicle's structure. The combined weight of the required coolant gas on board and its necessary storage structure may result in a high penalty in the payload capacity of a vehicle that utilises transpiration cooling as opposed to conventional thermal protection systems, e.g. ablative heat shields. To investigate the application of transpiration cooling on such vehicles, a thorough coolant mass budget calculation is necessary for the intended mission, which would also allow the determination of structural requirements to store the required amount of coolant gas.

Designing a transpiration cooling system to protect a hypersonic vehicle from heat or oxidation is a multi-variable problem and requires several thousands of iterations before an optimised design can be obtained. In particular, the ever-changing external flow conditions (e.g., pressure, temperature, velocity, etc.) on a hypersonic trajectory demand a point-by-point calculation over the flight duration during which the transpiration cooling system would be active. This makes such design processes prohibitively expensive and lengthy to complete with conventional boundary-layer solvers, even on high performance computers. Engineering correlations or analytical models provide a rapid and inexpensive method to perform these calculations, particularly for first approximation designs. The proposed analytical model is the first of its kind that can be used as a rapid design tool to predict the required coolant mass for a given trajectory and a film coverage requirement in terms of wall coolant concentration in laminar flows. It can also be used on board the vehicle for its systems to self-control the required coolant that needs to be injected at any point in its trajectory. To demonstrate the capability of the model, a mass budget calculation is performed for a generic hypersonic vehicle that requires up to 85% of coolant coverage to protect the wall surface against oxidation over a target distance downstream of a porous injector.

The analytical model is employed to calculate the required coolant mass and the associated storage volume for a transpiration-cooled hypersonic vehicle (see Fig. 7a). The total length of the vehicle is 16 m with a leading edge span of $b = 5$ m. A porous injector of length s and an area of $A = sb$ is situated downstream of the leading edge. The area up to

a length of x' downstream of the porous injector is to be protected by a coolant film with a concentration effectiveness of at least 85%, i.e. $\eta_c(x') \geq 0.85$. A generic trajectory with a flight duration of $t_{\text{flight}} = 1333$ s is selected (see Fig. 7b). The US Standard Atmosphere Model [27] is employed to calculate the static pressure and static temperature, both functions of altitude. For simplicity, it is assumed that the static and edge quantities are equal and the boundary layer around the vehicle is strictly laminar throughout the flight.

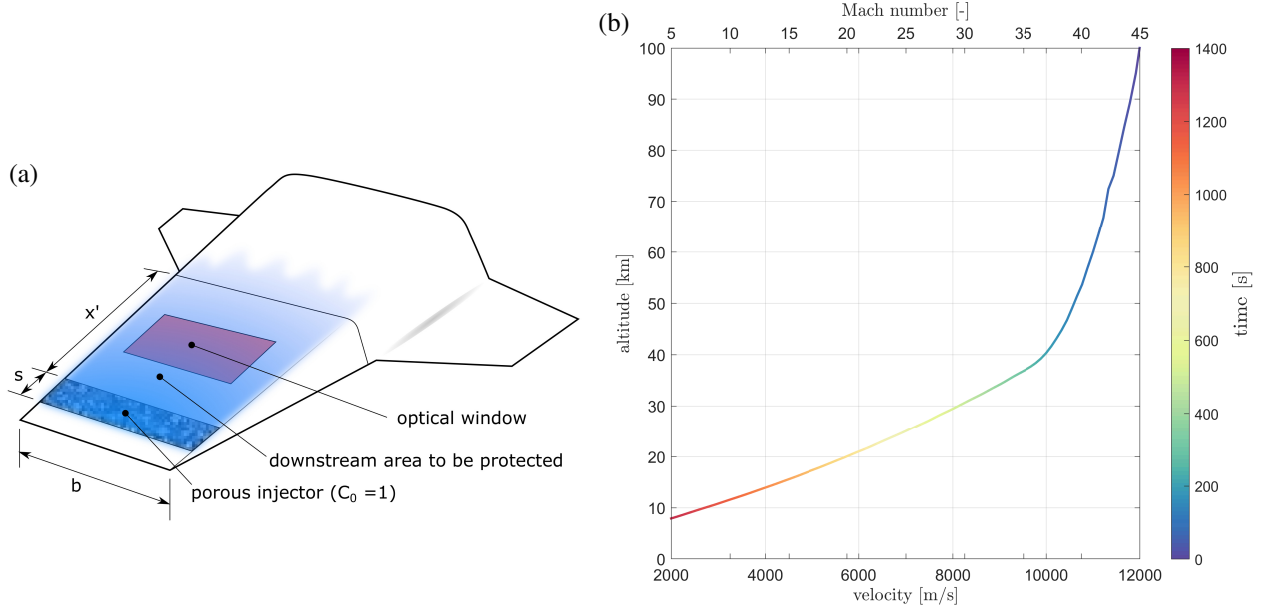


Fig. 7 (a) Schematic of a transpiration-cooled hypersonic vehicle (not to scale; coolant shown in blue) and (b) a generic trajectory of hypersonic flight.

The static temperature, static pressure, and velocity of the vehicle are substituted as T_e , p_e , and u_e , respectively, in Eq. (3) with the condition $\eta_c(x') \stackrel{!}{=} 0.85$. It is assumed that full coverage of the coolant exists on the porous injector, i.e. $C_0 = 1$. An isothermal wall temperature of $T_w = 2000$ K is assumed. The coolant is stored inside the vehicle at a pressure of $p_{\text{storage}} = 300$ bar and a temperature of $T_{\text{storage}} = 300$ K. Configurations with five different s values are calculated with a fixed value of $x' = 10$ m and another set of calculations are performed for five x' values with $s = 0.2$ m set as the injector length. For each configuration, the coolant gas is varied between nitrogen and helium. Equation 3 is subsequently solved for the blowing ratio, F , at each point on the trajectory. The coolant mass flow rate is obtained from the definition of blowing ratio and the continuity equation as follows:

$$\dot{m}_c = F \rho_e u_e A, \quad [\text{where } A = sb]. \quad (14)$$

The total coolant mass is determined by integrating Eq. (14) with respect to time, τ , expressed as a function of the flight duration, t_{flight} :

$$m_c(t_{\text{flight}}) = \int_0^{t_{\text{flight}}} \dot{m}_c d\tau. \quad (15)$$

Finally, the required volume for storing the coolant gas inside the vehicle is obtained from the equation

$$Q_{c, \text{storage}} = \frac{m_{c,t} R_G T_{\text{storage}}}{M_c p_{\text{storage}}}, \quad (16)$$

where $m_{c,t}$ is the total coolant mass required over the total flight duration of $t_{\text{flight}} = 1333$ s, i.e. $m_{c,t} = m_c(t_{\text{flight}} = 1333 \text{ s})$.

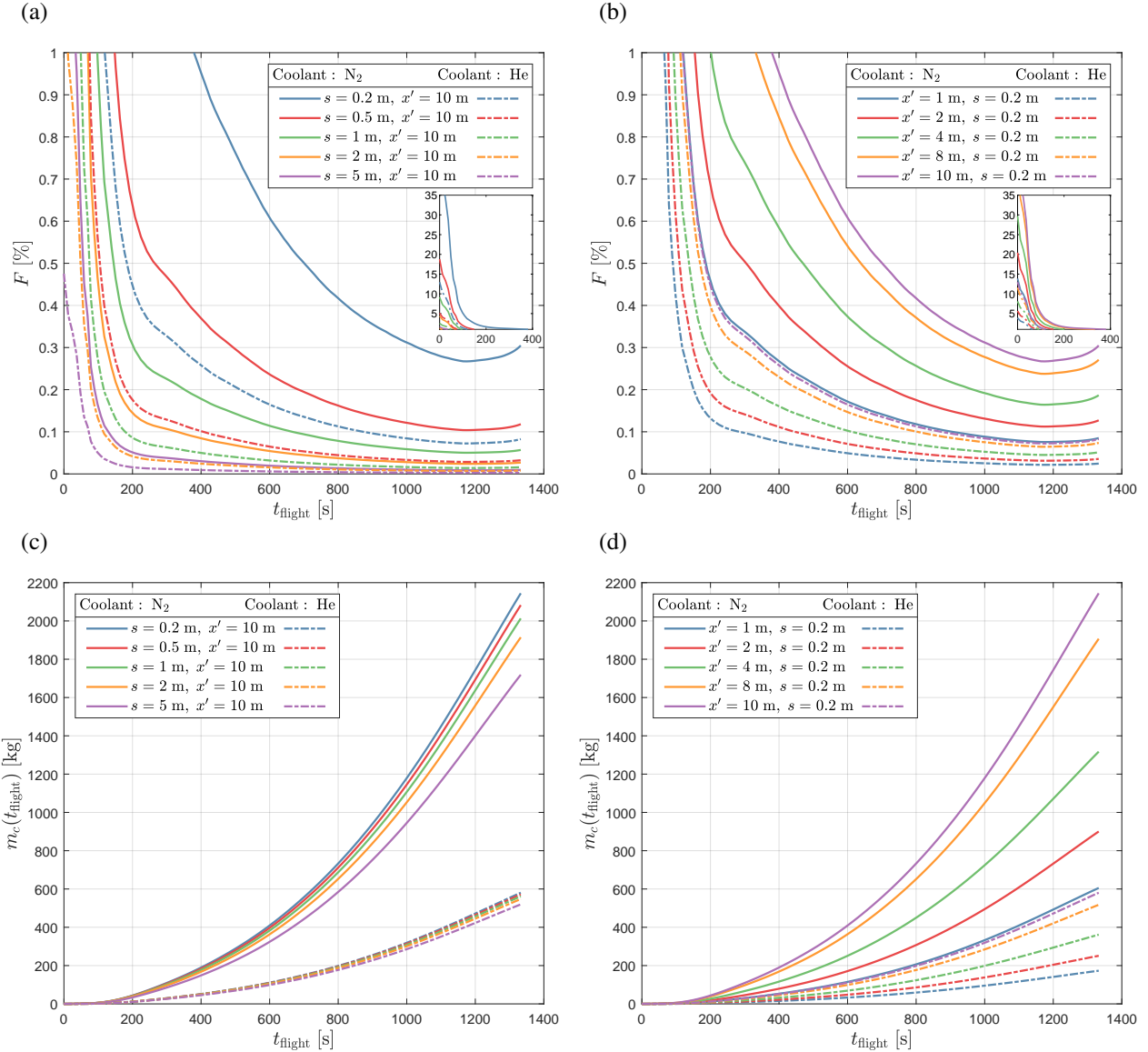


Fig. 8 Results of coolant mass budget calculation as a function of flight duration, t_{flight} . Required blowing ratio, F : variation in (a) s and (b) x' ; required coolant mass, m_c : variation in (c) s and (d) x' . F for flight duration up to $t_{\text{flight}} = 400$ s is plotted in the inset of subplots (a) and (b).

Results of the coolant mass budget calculation are presented in Fig. 8 and Table 2. When s is increased, the required blowing ratio, F , drops (see Fig. 8a), whereas larger values of x' result in higher F values (see Fig. 8b). The corresponding required coolant mass, m_c , is plotted in Figs. 8c and 8d, respectively for variations in s and x' . Analogous

Table 2 Required total coolant mass and volume for flight duration of 1333 s. Note: $x' = 10$ m when s is varied and $s = 0.2$ m when x' is varied.

Varied parameter	s [m]					x' [m]				
Input value	0.2	0.5	1	2	5	1	2	4	8	10
N ₂ , $m_{c,t}$ [kg]	2144.5	2082.7	2013.0	1914.5	1719.0	605.4	900.3	1317.2	1906.9	2144.5
He, $m_{c,t}$ [kg]	580.4	571.6	561.6	547.5	519.6	173.2	251.2	361.5	517.5	580.4
Ratio [-]	3.7	3.6	3.6	3.5	3.3	3.5	3.6	3.6	3.7	3.7
N ₂ , $Q_{c,storage}$ [m ³]	6.4	6.2	6.0	5.7	5.1	1.8	2.7	3.9	5.7	6.4
He, $Q_{c,storage}$ [m ³]	12.1	11.9	11.7	11.4	10.8	3.6	5.2	7.5	10.8	12.1
Ratio [-]	0.53	0.52	0.51	0.50	0.47	0.50	0.51	0.52	0.53	0.53

to the blowing ratio, F , the required coolant mass, m_c , decreases with higher s values (Fig. 8c) and the opposite trend can be noticed when x' is increased (Fig. 8d). According to Eq. (10), the coolant's initial slab height, h , thickens when s is increased, and this results in a higher value of the driving parameter, ζ , and therefore η_c , as discussed in Section III. Thus, the required coolant concentration of at least $\eta_c = 85\%$ is achieved with a lower F as s is increased. On the other hand, as x' increases, ζ and η_c drop (note: $x' = x - x_0$), and a higher F is required to maintain the criterion of $\eta_c \geq 85\%$. For a given point in time (t_{flight}), the required coolant mass (Eq. 15) follows the same trend as F for variations in both s and x' (compare Figs. 8c and 8d to Figs. 8a and 8b) since $m_c \propto F$ when the product $\rho_e u_e A$ is constant according to Eq. (14).

For a given set of s and x' , the blowing ratio decreases as the flight progresses up until $t_{flight} \approx 1150$ s (see Figs. 8a and 8b). After this point in time, the required blowing ratio increases. This is due to the different pressure and temperature distributions in the troposphere starting at an altitude of 11 km (see Fig. 7b). This demonstrates the proposed model's ability to easily take these drastic, non-monotonic changes in the flow conditions into account. It can be further seen in Figs. 8a and 8b that the blowing ratios range from 1% to 35% within the first 400 s of flight (see inset). However, the required total coolant mass is significantly smaller (see Figs. 8c and 8d) – compared to the mass required over the flight duration that follows – despite the high blowing ratios during this time period. This is because the edge mass flux, $\rho_e u_e$, at these altitudes is relatively low due to the low density in the atmosphere. In other words, the oxygen partial pressure is significantly lower at these altitudes, and therefore only a small amount of coolant gas is required to protect the vehicle's surface from oxidation. As the vehicle descends, the density of the atmosphere rises and the required F value drops. According to Eq. (14), however, a higher coolant mass flow rate is needed as the air density, ρ_e , rises drastically.

Fig. 8 further illustrates the efficiency of helium as a protective film. For every variation – as expected – helium forms a better film coverage for significantly lower total mass compared to nitrogen as the coolant gas (see Figs. 8c and 8d). The required total coolant mass for the full flight duration of $t_{flight} = 1333$ s, denoted as $m_{c,t}$, is given in Table 2 for all variations in s and x' . On an average, 3.6 times less coolant mass is needed when helium is used instead of

nitrogen ($m_{c,t,N_2}/m_{c,t,He} = 3.6$). Note that this effect is not identical to the commonly reported higher thermal film effectiveness of helium. A higher thermal film effectiveness stems from the large heat capacity of helium, which has been reported in numerous studies (e.g. Richards and Stollery [14], Meinert et al. [28], and Langener et al. [29]). In the current analysis, it is shown that a similar effect is achieved by strictly considering the coolant's concentration effectiveness at the wall. The thermal and concentration-based effects are connected through the molar mass of the coolant [28], and the proposed model is able to delineate the role of the coolant's molar mass in forming the physical film with respect to its concentration and, consequently, in its final cooling performance.

The required coolant storage volume, $Q_{c, storage}$, over the full flight duration of $t_{flight} = 1333$ s is given in Table 2. For the required coolant mass, the coolant storage volume needed for nitrogen is, on average, half of that needed for helium ($Q_{c, storage, N_2}/Q_{c, storage, He} = 0.51$). Evaluating Eq. (16) for nitrogen and helium and subsequently constructing the ratio thereof yields

$$\frac{Q_{c, storage, N_2}}{Q_{c, storage, He}} = \frac{m_{c,t, N_2}}{m_{c,t, He}} \frac{M_{He}}{M_{N_2}}. \quad (17)$$

With the ratios $m_{c,t, N_2}/m_{c,t, He} = 3.6$ (from Table 2) and $M_{N_2}/M_{He} = 7$, the ratio $Q_{c, storage, N_2}/Q_{c, storage, He} = 0.51$ is obtained. For the same mass as nitrogen, i.e. $m_{c,t, N_2}/m_{c,t, He} = 1$, helium would occupy seven times more volume than nitrogen since $Q_{c, storage, He} = 7Q_{c, storage, N_2}$ according to Eq. (17). Similarly, helium forms a more formidable film once injected due to its seven times higher volumetric flow rate at a given mass flow rate as discussed by Ifti et al. [3], Gülhan and Braun [19], Keller et al. [17], and Hombsch and Olivier [16].

The required coolant storage volume, $Q_{c, storage}$, is a significant design parameter for the coolant's storage structure and the vehicle's overall volume. In practice, the coolant would be contained at a constant temperature ($T_{storage}$) inside the vehicle in a pressure vessel that would be limited by a maximum pressure ($p_{storage}$). This means a lighter gas, i.e. a gas with lower molar mass, M_c , would result in a higher total coolant volume, $Q_{c, storage}$, for a given $m_{c,t}$ (see Eq. 16). The mixing – as predicted by the proposed model – would dictate how large $m_{c,t}$ has to be for a given coolant gas and a target concentration effectiveness, η_c . Although $T_{storage}$ and $p_{storage}$ can be varied theoretically, in practice the variation would be possible only within a narrow range. $T_{storage}$ has to be close to the vehicle's internal temperature, and increasing $p_{storage}$ to reduce the storage volume would require strengthening of the structure, which would add to the total weight of the vehicle.

For the calculated configurations (Table 2), the storage volume required for helium is approximately twice the storage volume needed for nitrogen. Helium's higher volumetric flow rate – an advantageous property that helps form a better film with a lower mass requirement – becomes a disadvantage for the vehicle's overall volume. It is, therefore, necessary to determine both the required total coolant mass and total coolant storage volume to design a vehicle that utilises transpiration cooling. Both of these critical design parameters can be obtained by using the proposed model.

The analytical model presented in this article can be employed to rapidly perform these coolant mass budget

calculations without the need of any significant computational power by simply using the trajectory data, and critical design parameters such as s and x' can be easily varied as demonstrated here. Thousands of iterations of these inexpensive calculations can be performed rapidly to find the optimal design parameters for a given mission.

V. Conclusion

Although numerous prediction models exist for predicting the mixing between the coolant film and the boundary-layer gas in turbulent flows, such models are not widely available for laminar flows. In particular, no model exists that describes the mixing process in terms of the coolant concentration, which is important for laminar flows where the heat and mass transfer analogy does not apply. The coolant concentration is the core parameter for successfully designing an oxidation protection system. In this study, an analytical model based on one-dimensional diffusion is proposed to predict laminar mixing of the coolant at the wall downstream of the injector in terms of concentration. The model is validated against experimental data obtained at Mach 7 employing nitrogen and helium as the coolant gas over a flat-plate. The analytical results match the experimental data within 17% and correctly predict the slope of the monotonic decay of the coolant concentration. The model further describes the role of variables such as stream-wise velocity, diffusion coefficient, and blowing ratio in the mixing process. A coolant mass budget calculation performed for a transpiration-cooled hypersonic vehicle descending on a generic trajectory shows that using helium as the coolant gas requires 3.6 times less mass when compared to configurations where nitrogen is employed as the coolant, demonstrating the efficiency of helium in forming a protective film downstream of the injector. However, helium requires twice the storage volume when compared to nitrogen, a factor that has to be accounted for – if the efficiency of helium is to be exploited – when designing a vehicle. Lowering the required coolant mass by using a lighter gas such as helium could come at a cost of a higher overall volume requirement. The proposed analytical model is a useful tool for rapidly performing mass budget calculations to design transpiration cooling systems on supersonic and hypersonic vehicles. The model could also be implemented on board a vehicle to enable a self-controlling system. In particular, the model's prediction of coolant concentration can be directly used to design an oxidation protection system. The concentration distribution obtained from this model could be further employed to improve existing film cooling correlations for laminar flows. Foremost, however, this model explains the mixing mechanism between the coolant film and the boundary-layer gas at the wall in a laminar flow; it is demonstrated that this mixing mechanism at the wall is driven by diffusion.

Acknowledgements

The funding for this research by the Engineering and Physical Sciences Research Council (EPSRC) grant 'Transpiration Cooling Systems for Jet Engine Turbines and Hypersonic Flight' (reference: EP/P000878/1) is gratefully acknowledged. The authors would like to thank Dr James Merrifield of Fluid Gravity Engineering Ltd. for his help with TINA simulations and Dr Markus Kloker for the discussion on cooling effectiveness.

References

- [1] van Driest, E. R., "The Problem of Aerodynamic Heating," *Aeronautical Engineering Review*, Vol. 15, No. 10, 1956, pp. 26–41.
- [2] Anderson, J. J. D., *Hypersonic and High-Temperature Gas Dynamics, Second Edition*, American Institute of Aeronautics and Astronautics, Reston, VA, 2006. <https://doi.org/10.2514/4.861956>.
- [3] Ifiti, H. S., Hermann, T., Ewenz Rocher, M., Doherty, L., Hambidge, C., McGilvray, M., and Vandeperre, L., "Laminar transpiration cooling experiments in hypersonic flow," *Experiments in Fluids*, Vol. 63, No. 6, 2022, pp. 1–14. <https://doi.org/10.1007/s00348-022-03446-1>.
- [4] Ifiti, H. S., Hermann, T., McGilvray, M., Larrimbe, L., Hedgecock, R., and Vandeperre, L., "Flow Characterization of Porous Ultra-High-Temperature Ceramics for Transpiration Cooling," *AIAA Journal*, Vol. 60, No. 5, 2022. <https://doi.org/10.2514/1.J061009>.
- [5] Ewenz Rocher, M., McGilvray, M., Hermann, T. A., Ifiti, H. S., Hufgard, F., Eberhart, M. F., Meindl, A., Loehle, S., Giovannini, T., and Vandeperre, L. J., "Testing a Transpiration Cooled Zirconium-Di-Boride sample in the Plasma Tunnel at IRS," *AIAA Scitech 2019 Forum*, American Institute of Aeronautics and Astronautics, Reston, Virginia, 2019, p. 01. <https://doi.org/10.2514/6.2019-1552>.
- [6] Tropf, W. J., Thomas, M. E., Harris, T. J., and Lutz, S. A., "Performance of Optical Sensors in Hypersonic Flight," *Johns Hopkins APL Technical Digest*, Vol. 8, No. 4, 1987.
- [7] Giles, D. N., "Integral cooling system for high-temperature missile structures," , Apr. 1988.
- [8] Goldstein, R. J., "Film Cooling," *Advances in Heat Transfer*, Vol. 7, 1971, pp. 321–379. [https://doi.org/10.1016/S0065-2717\(08\)70020-0](https://doi.org/10.1016/S0065-2717(08)70020-0).
- [9] Fujiwara, K., Sriram, R., Kontis, K., and Ideta, T., "Review on Film Cooling in High-Speed Flows," *31st International Symposium on Shock Waves 2*, Springer, Cham, 2017, pp. 939–946. https://doi.org/10.1007/978-3-319-91017-8_118.
- [10] Fitt, A. D., Ockendon, J. R., and Jones, T. V., "Aerodynamics of Slot-Film Cooling: Theory and Experiment," *Journal of Fluid Mechanics*, Vol. 160, 1985, pp. 15–27. <https://doi.org/10.1017/S0022112085003366>.
- [11] Yavuzkurt, S., Moffat, R. J., and Kays, W. M., "Full-Coverage Film Cooling. Part 1. Three-Dimensional Measurements of Turbulence Structure," *Journal of Fluid Mechanics*, Vol. 101, No. 1, 1980, pp. 129–158. <https://doi.org/10.1017/S0022112080001577>.
- [12] Yavuzkurt, S., Moffat, R. J., and Kays, W. M., "Full-Coverage Film Cooling. Part 2. Prediction of the Recovery-Region Hydrodynamics," *Journal of Fluid Mechanics*, Vol. 101, No. 1, 1980, pp. 159–178. <https://doi.org/10.1017/S0022112080001589>.
- [13] Hermann, T., McGilvray, M., and Naved, I., "Performance of Transpiration-Cooled Heat Shields for Reentry Vehicles," *AIAA Journal*, 2019. <https://doi.org/10.2514/1.J058515>.
- [14] Richards, B. E., and Stollery, J. L., "Laminar Film Cooling Experiments in Hypersonic Flow," *Journal of Aircraft*, 1979. <https://doi.org/10.2514/3.58502>.

- [15] Heufer, K. A., and Olivier, H., “Experimental and Numerical Study of Cooling Gas Injection in Laminar Supersonic Flow,” *AIAA Journal*, 2008. <https://doi.org/10.2514/1.34218>.
- [16] Hombsch, M., and Olivier, H., “Film Cooling in Laminar and Turbulent Supersonic Flows,” *Journal of Spacecraft and Rockets*, 2013. <https://doi.org/10.2514/1.A32346>.
- [17] Keller, M. A., Kloker, M. J., and Olivier, H., “Influence of Cooling-Gas Properties on Film-Cooling Effectiveness in Supersonic Flow,” *Journal of Spacecraft and Rockets*, 2015. <https://doi.org/10.2514/1.A33203>.
- [18] Kays, W. M., Crawford, M. E., and Weigand, B., *Convective Heat and Mass Transfer*, 4th ed., McGraw-Hill Higher Education, 2005.
- [19] Gülhan, A., and Braun, S., “An experimental study on the efficiency of transpiration cooling in laminar and turbulent hypersonic flows,” *Experiments in Fluids*, Vol. 50, No. 3, 2010, pp. 509–525. <https://doi.org/10.1007/s00348-010-0945-6>.
- [20] Crank, J., *The Mathematics of Diffusion*, 2nd ed., Oxford University Press, 1979.
- [21] Bird, R. B., Stewart, W. E., and Lightfoot, E. N., *Transport Phenomena*, 2nd ed., John Wiley & Sons, New York, 2007.
- [22] Blasius, H., “Grenzschichten in Flüssigkeiten mit kleiner Reibung,” *Zeitschrift für angewandte Mathematik und Physik*, Vol. 56, 1908, pp. 1–37.
- [23] Netterfield, M. P., “Validation of a Navier Stokes Code for Thermochemical Non Equilibrium Flows,” *AIAA Twenty-Seventh Thermophysics Conference*, 1992.
- [24] Netterfield, M. P., “Hypersonic Aerothermodynamic Computations Using a Point - Implicit TVD Method,” *First European Symposium on Aerothermodynamics for Space Vehicles, ESTEC*, 1991.
- [25] Ifiti, H. S., Hermann, T., McGilvray, M., and Merrifield, J., “Numerical Simulation of Transpiration Cooling in a Laminar Hypersonic Boundary Layer,” *Journal of Spacecraft and Rockets*, 2022. <https://doi.org/10.2514/1.A35325>.
- [26] Eckert, E. R. G., “Engineering Relations for Heat Transfer and Friction in High-Velocity Laminar and Turbulent Boundary-Layer Flow over Surfaces with Constant Pressure and Temperature,” *Transactions of the American Society of Mechanical Engineers*, Vol. 78, No. 6, 1956, p. 1273.
- [27] “U.S. Standard Atmosphere,” U.S. Government Printing Office, 1976.
- [28] Meinert, J., J-ogrove, Huhn, R. G., Serbest, E., and Haidn, O. J., “Turbulent Boundary Layers with Foreign Gas Transpiration,” *Journal of Spacecraft and Rockets*, Vol. 38, No. 2, 2001, pp. 191–198. <https://doi.org/10.2514/2.3693>.
- [29] Langener, T., Wolfersdorf, J. V., and Steelant, J., “Experimental Investigations on Transpiration Cooling for Scramjet Applications Using Different Coolants,” *AIAA Journal*, Vol. 49, No. 7, 2011, pp. 1409–1419. <https://doi.org/10.2514/1.J050698>.